Available online at www.sciencedirect.com
ScienceDirect
Journal of Sound and Vibration 302 (2007) 409–424
JOURNAL OF SOUND AND VIBRATION
www.elsevier.com/locate/jsvi

A theoretical and experimental study of advanced control methods to suppress vibrations in a small square plate subject to temperature variations

P. Shimon, Y. Hurmuzlu*

Department of Mechanical Engineering, Southern Methodist University, P.O. Box 750337, Dallas, TX 75275, USA

Received 24 March 2003; received in revised form 7 January 2005; accepted 26 January 2005
Available online 1 February 2007

Abstract

In this paper, we seek to develop an efficient controller for vibration reduction in a small square plate clamped on all edges. The plate mimics a piece of an aircraft's skin. Small plate size results in higher natural frequencies than normally investigated in literature. Such high-frequency systems are more susceptible to time delays. In addition, the control system must be able to operate over a wide range of temperatures, a requirement for in-flight vibration suppression systems. We investigate two methodologies (sliding mode control, and an adaptive H_∞ control) for control over a wide range of temperatures. Theoretical and experimental studies are conducted and produced varying results. The best theoretical and experimental results are obtained with the adaptive H_∞ controller.

1. Introduction

Acoustical fatigue in aircraft fuselage panels can be minimized when an aircraft is designed. With a proper aerodynamic design, turbulent flow across the fuselage can be minimized. When an existing aircraft is modified to serve another purpose, the airframe is often changed (such as adding a radar pod). The resulting change can create turbulent airflow around the fuselage and acoustical fatigue becomes more of a concern.

This paper continues the work in Ref. [1] where an H_∞ controller using a distributed strain actuator was able to suppress the vibrations in a thin (0.81 mm) 152.4 mm square aluminum plate. In this paper a thin (1.2 mm) 203.2 mm square aluminum plate is studied and only the first three modes of vibration are considered.

The first step was to investigate the variations in the dynamics of the plate and actuator due to temperature changes. The temperature dependency of the system in an open-loop configuration was investigated. This was performed by exciting a set of distributed strain actuators attached to the plate. A range of temperatures that vary from -50 to $75\,^{\circ}C$ was considered.

*Corresponding author. Tel.: +1 214 768 3498; fax: +1 214 768 1473.
E-mail address: hurmuzlu@seas.smu.edu (Y. Hurmuzlu).

0022-460X/$ - see front matter © 2005 Elsevier Ltd. All rights reserved.
doi:10.1016/j.jsv.2005.01.054

Next, two control systems were developed to suppress vibrations over the temperature range: an adaptive H_∞ controller, and a sliding mode controller. These controllers were developed to suppress the vibrations for the first three modes.

Finally, the closed-loop system was tested from -25 to $50\,^\circ$C. A positive velocity controller (PVF) was used as a baseline for performance. The controllers were tuned at $-25\,^\circ$C because system noise has the greatest effect at that temperature.

2. Plate modeling

The dynamics equation for a fully clamped plate is given as

$$D\left(\frac{\partial^2 W(x,y)}{\partial x^4}+2\frac{\partial^4 W(x,y)}{\partial x^2 y^2}+\frac{\partial^4 W(x,y)}{\partial y^4}\right)-\rho h\omega^2 W(x,y)=0. \tag{1}$$

From Ref. [2], the displacement function of a clamped plate is

$$W(x,y)=\sum_{n=1}^{N}\xi_i W_i(x,y),\quad i=1,\ldots, \tag{2}$$

where $W_i(x,y)$ is the coordinate function for the ith mode, and ξ_i is the modal coefficient for the ith mode. The coordinate functions for the first three modes are chosen as (see Ref. [3])

$$W_1(x,y)=(\alpha_1 x^4+\beta_1 x^2+1)(\alpha_1 y^4+\beta_1 y^2+1), \tag{3a}$$

$$W_2(x,y)=x(\alpha_2 x^4+\beta_2 x^2+1)(\alpha_2 y^4+\beta_2 y^2+1), \tag{3b}$$

$$W_3(x,y)=y(\alpha_3 x^4+\beta_3 x^2+1)(\alpha_3 y^4+\beta_3 y^2+1). \tag{3c}$$

From the boundary conditions one can determine the coefficients α_i and β_i for a square plate with elastically restrained edges as

$$\alpha_1=\frac{16(a+2D\phi)}{a^4(a+10D\phi)},\quad \beta_1=-\frac{8(a+6D\phi)}{a^2(a+10D\phi)}, \tag{4a}$$

$$\alpha_2=\alpha_3=\frac{16(a+6D\phi)}{a^4(a+14D\phi)},\quad \beta_2=\beta_3=-\frac{8(a+10D\phi)}{a^2(a+14D\phi)}, \tag{4b}$$

where $a=b$ for a square plate.

Given the dynamics equation (1), and the coordinate functions (2), we can use Galerkin's method to solve for the natural frequencies in terms of the plates physical characteristics and boundary conditions (see Ref. [4]). By experimentally measuring the first modal frequency of the 203.2 mm square plate, $\phi=\phi_x=\phi_y$ was determined to be 0.0014. The first three modal frequencies are shown in Table 1. ξ_i is found by normalizing the coordinate functions:

$$\int_{-\frac{a}{2}}^{\frac{a}{2}}\int_{-\frac{a}{2}}^{\frac{a}{2}}\rho W_{mn}(x,y)W_{mn}(x,y)\,\mathrm{d}x\,\mathrm{d}y=1,\quad n=1,2,\ldots\ . \tag{5}$$

For the given plate, ξ_i was found to be 10.45, 317.22, and 317.22 for the first three modes. Fig. 1 shows the mode shapes for the first three modes.

Table 1
Eigenvalues and modal frequencies

n	ω_i	c_i
1	1351.39	90
2	2872.80	100
3	2872.80	100

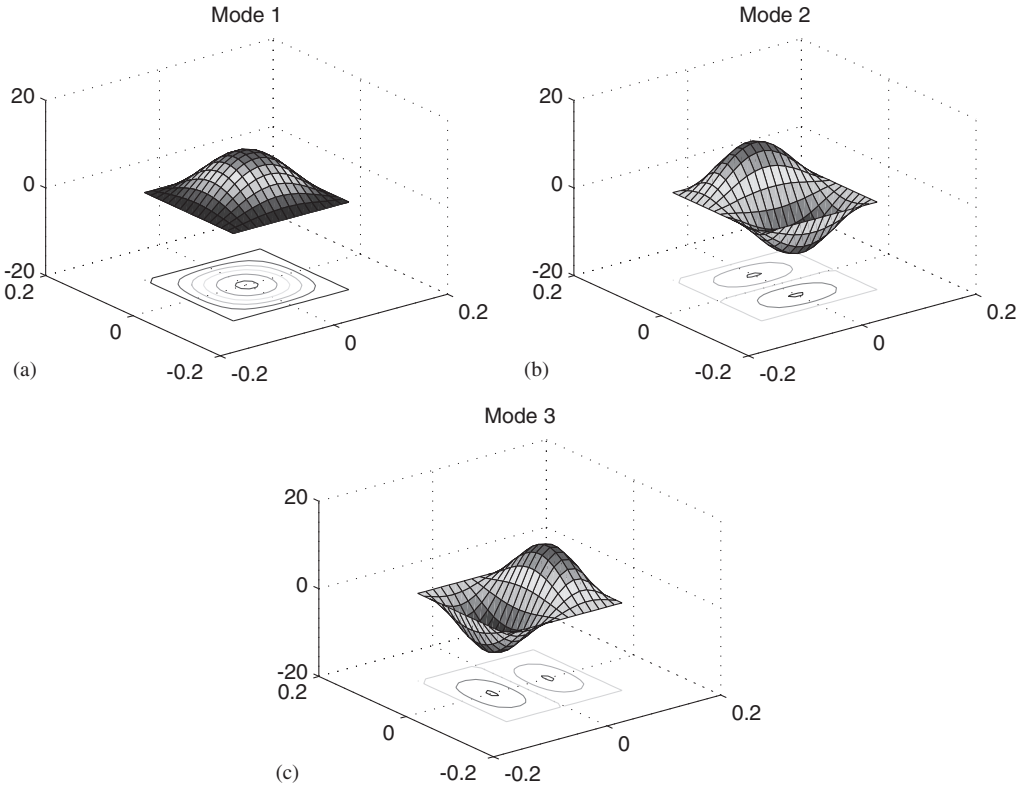

Fig. 1. Mode shapes of a square plate clamped on all sides: (a) Mode 1, (b) Mode 2, (c) Mode 3.

With the modal frequencies and shapes known, the forced vibration of the plate can be expressed as

$$\ddot{\eta}_i(t) + c_i\dot{\eta}_i(t) + \omega_i^2\eta_i(t) = N_i(t), \quad i = 1, 2, \ldots . \tag{6}$$

In the above equations $N_i(t)$ are the external forces, ω_i are the modal radial frequencies, and c_i are the damping coefficients (determined experimentally, see Section 3.1). Table 1 shows the values for the first three modes.

The actuator used in this investigation is a distributed strain actuator (patch). The actuator is a thin layer of piezoelectric material that is directly bonded to the plate. With an actuator bonded to the plate equation (6) becomes

$$\eta_i'' + c_i\dot{\eta}_i + \omega^2\eta_i = \gamma_i v_i, \tag{7}$$

where γ_i is the actuator gain.

3. Adaptive control for model uncertainty

In this section, the effects caused by temperature and imperfect bonding of the patch to the plate are investigated. These effects can cause significant error in the model if not accounted for.

3.1. Problem description

The model for the plate used in the control design assumes that the system is operating at room temperature and that the piezoelectric material of the patch is perfectly bonded to the plate (see Eq. (6)). In reality, the system needs to operate over a wide range of temperatures and the patch is not perfectly bonded. The two effects cause the constant parameter γ to vary in a nonlinear fashion.

3.1.1. Imperfect bonding

The distributed strain actuator used in the system has a polyamide coating around the piezoelectric material. This coating provides protection to the piezoelectric material, but prevents the material from being bonded directly to the plate. As a result, the force γ is reduced. In order to model this correctly, the material properties of the polyamide would need to be known and a more complex model would need to be developed. However, in this study an adaptive controller was implemented to account for the imperfect bonding effect.

3.1.2. Temperature effects

This system needs to be able to operate over a wide range of temperatures. High temperatures can be present just after the aircraft takes off and low temperatures are present when the aircraft is in flight at high altitudes. The piezoelectric material has a nonlinear dependence on temperature. As the temperature drops, there is a slight drop in performance until 0 °C is reached. Further drops in temperature would dramatically affect the performance of the actuator (as per manufactures specifications).

The polyamide coating of the distributed strain actuators offers another level of uncertainty. As the temperature drops, the material hardens and creates a stiffer bond to the plate. This causes the actuator performance to improve as the temperature drops, the opposite effect of piezoelectric material. The combination of these two effects made the modeling of the actuator performance due to temperature effects very difficult. Again, the adaptive controller was used to account for the variations instead of extensive modeling of the polyamide material (something not possible because the material properties of the polyamide were not available from the manufacturer).

3.2. Parameter identification

Since all of the uncertainties manifest in one parameter, a parameter identification method can be used. One can safely assume that the parameter will vary slowly over time because the variation is due to temperature changes. A least-squares method was used to compensate for noise in the system. This method is suitable because it averages out measurement noise.

The design of the least-squares method is straightforward and adopted from Sastry and Bodson [5]. From Eq. (7), the model of the system is

$$\eta_i'' + C_i\dot{\eta}_i + \omega^2\eta_i = \gamma_i^* v_i, \tag{8}$$

where γ_i^* is the unknown actual actuator gain. In this approach the integral squared error is minimized,

$$\mathrm{ISE} = \int_0^t e_1^2(\tau)\,\mathrm{d}\tau, \tag{9}$$

where the error (e_i) is defined as

$$e_i = \gamma_i v_i(t) - \gamma_i^* v_i(t) \tag{10}$$

or

$$e_i = \gamma_i v_i(t) - (\eta_i''(t) + c_i\dot{\eta}_i(t) + \omega^2\eta_i(t)). \tag{11}$$

Defining $y_i(t) = \eta_i''(t) + c_i\dot{\eta}_i(t) + \omega^2\eta_i(t)$, Eq. (11) becomes

$$e_i = \gamma_i v_i(t) - y_i(t). \tag{12}$$

The parameter γ_i can be determined by setting the derivative of the error with respect to γ_i to zero:

$$\frac{\partial}{\partial\gamma_i}\left(\int_0^t e_i^2(\tau)\,\mathrm{d}\tau\right) = 2\int_0^t (v_i(\tau)(\gamma_i v_i(\tau) - y_i(\tau)))\,\mathrm{d}\tau = 0. \tag{13}$$

Therefore,

$$\gamma_i(t) = \left(\int_0^t v_i(\tau)^2\,\mathrm{d}\tau\right)^{-1}\left(\int_0^t v_i(\tau)y_i(\tau)\,\mathrm{d}\tau\right). \tag{14}$$

As long as persistent excitation exists, $v_i(t)$ will not equal zero and

$$\left(\int_0^t v_i(\tau)^2\,\mathrm{d}\tau\right)^{-1} \to 0, \tag{15}$$

therefore, γ_i will be bounded and approach γ_i^*.

The system needs to be implemented in real time so a recursive formulation has to be developed [6]. Define

$$P_i(t) = \left(\int_0^t v_i(\tau)^2\,\mathrm{d}\tau\right)^{-1}. \tag{16}$$

Then

$$\frac{\mathrm{d}}{\mathrm{d}t}(P_i(t)^{-1}) = v_i(t)^2. \tag{17}$$

It can be shown that

$$\begin{aligned} 0 &= \frac{\mathrm{d}}{\mathrm{d}t}(P_i(t)P_i(t)^{-1}) \\ &= \frac{\mathrm{d}}{\mathrm{d}t}(P_i(t))P_i(t)^{-1} + P_i(t)\frac{\mathrm{d}}{\mathrm{d}t}(P_i(t)^{-1}). \end{aligned} \tag{18}$$

Eq. (18) can be rewritten as

$$\begin{aligned} \frac{\mathrm{d}}{\mathrm{d}t}(P_i(t)) &= -P_i(t)^2\frac{\mathrm{d}}{\mathrm{d}t}(P_i(t)^{-1}) \\ &= -P_i(t)^2 v_i(t)^2. \end{aligned} \tag{19}$$

From Eqs. (14) and (16) it can be shown that

$$\gamma_i(t) = P_i(t)\left(\int_0^t v_i(\tau)y_i(\tau)\,\mathrm{d}\tau\right). \tag{20}$$

Thus,

$$\begin{aligned} \frac{\mathrm{d}}{\mathrm{d}t}\gamma_i(t) &= \frac{\mathrm{d}}{\mathrm{d}t}P_i(t)\left(\int_0^t v_i(\tau)y_i(\tau)\,\mathrm{d}\tau\right) + P_i(t)v_i(t)y_i(t) \\ &= -P_i(t)^2 v_i(t)^2\gamma_i(t)P_i(t)^{-1} + P_i(t)v_i(t)y_i(t) \\ &= -P_i(t)v_i(t)(\gamma_i(t)v_i(t) - y_i(t)). \end{aligned} \tag{21}$$

To control the convergence rate of γ_i to γ_i^*, a constant $g>0$ is introduced. So,

$$\dot{P}_i(t) = -gP_i(t)^2 v_i(t)^2, \tag{22}$$

$$\dot{\gamma}_i(t) = -gP_i(t)v_i(t)(\gamma_i(t)v_i(t) - y_i(t)). \tag{23}$$

As long as $P_i(0)>0$, the convergence scheme will be bounded.

The least-squares method is very good at noise rejection, however, it does not allow for the parameter to vary over time because $P_i(t) \to 0$, and stops γ_i from adapting. This can handle this in two ways: first, $P_i(t)$ can be reset at specific times, for example when the temperature changes 5° and the second option is to add a forgetting factor [6] in the form of

$$\dot{P}_i(t) = g\lambda_a P_i(t) - gP_i(t)^2 v_i(t)^2, \tag{24}$$

where $\lambda_a>0$. The utility of each approach was studied in the testing phase.

Table 2
Parameter values for the adaptive temperature test

Temp (°C)	Persistent excitation				LSw/FF
	15 V	30 V	15 V w/noise	30 V w/noise	30 V w/noise
−50	9.3×10^{-3}	9.1×10^{-3}	9.0×10^{-3}	9.0×10^{-3}	10.1×10^{-3}
−36	10.9×10^{-3}	10.4×10^{-3}	10.6×10^{-3}	10.2×10^{-3}	11.1×10^{-3}
−22	11.9×10^{-3}	12.5×10^{-3}	11.8×10^{-3}	12.0×10^{-3}	11.9×10^{-3}
−12	14.6×10^{-3}	14.7×10^{-3}	14.1×10^{-3}	14.2×10^{-3}	13.9×10^{-3}
1	15.6×10^{-3}	16.1×10^{-3}	15.5×10^{-3}	15.7×10^{-3}	15.4×10^{-3}
2.5	15.3×10^{-3}	15.7×10^{-3}	15.0×10^{-3}	15.1×10^{-3}	NA
11.5	13.2×10^{-3}	14.0×10^{-3}	13.0×10^{-3}	12.7×10^{-3}	12.3×10^{-3}
13.5	12.9×10^{-3}	12.9×10^{-3}	12.7×10^{-3}	13.0×10^{-3}	NA
18.5	14.7×10^{-3}	15.3×10^{-3}	NA	NA	NA
22.5	12.7×10^{-3}	12.5×10^{-3}	NA	NA	NA
25	16.1×10^{-3}	16.1×10^{-3}	NA	NA	15.9×10^{-3}
38.5	13.2×10^{-3}	13.2×10^{-3}	13.2×10^{-3}	13.6×10^{-3}	13.5×10^{-3}
50	14.0×10^{-3}	13.7×10^{-3}	13.7×10^{-3}	14.2×10^{-3}	14.5×10^{-3}
62	12.6×10^{-3}	12.7×10^{-3}	12.7×10^{-3}	12.9×10^{-3}	12.9×10^{-3}
75	12.7×10^{-3}	12.8×10^{-3}	12.9×10^{-3}	13.4×10^{-3}	13.4×10^{-3}

3.3. Implementation of the adaptive controller

In simulation, the adaptive controller was able to predict the parameter as long as there was a persistent excitation. The simulations results are not presented because they do not add significantly to the content of the article. The next step was to test the adaptive controller in the actual system (see Section 5 for the experimental setup). The controller was implemented using the 152.4 mm square plate and was tested over a wide range of temperatures. The test was performed five times. The first four used the standard least-squares implementation with four different persistent excitations. The patch was excited with either a 15 or 30 V, 100 Hz sine wave and with or without noise applied in the form of air flow over the plate. The fifth test used the least-squares algorithm with a forgetting factor (LSw/FF), persistently excited by a 30 V, 100 Hz sine wave with noise. In all cases $g = 0.001$ and in the fifth case, $\lambda_a = 0.001$. Table 2 shows the results of the test. The validity of the tabulated results will be verified through controller performance.

4. Advance control design for three modes

In this section, two controllers are proposed, an H_∞ controller with adaptive parameter estimation and a sliding mode controller. The controllers are designed to suppress the vibrations for the first four modes of an 203.2 mm square plate. The H_∞ controller is a robust linear controller that can account for the uncertainties in the model. To account for the temperature and bonding nonlinearities, an adaptive controller is added. This controller effectively linearizes the system so that the linear H_∞ controller can be used. The sliding mode controller is a nonlinear controller that will account for both model uncertainties and nonlinearities due to bonding and temperature effects.

4.1. Problem description

There are three actuators being used to control the first three modes of vibration. See Fig. 2 for a picture of the plate with actuator and accelerometer locations. The location of the actuators were chosen to minimize the number of modes each actuator would excite. As a result the first actuator only affects the first mode, the second and third actuators affect the second and first modes and third and first modes, respectively.

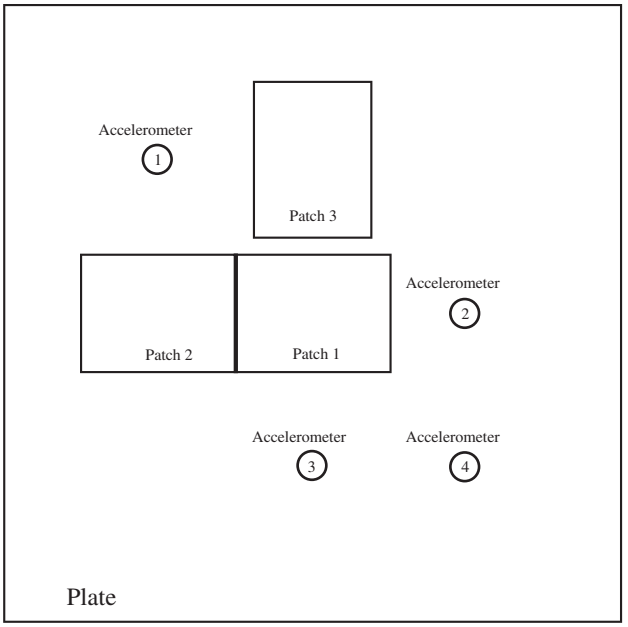

Fig. 2. Patch and accelerometer placement.

With the locations of the actuators decided, Eq. (6) can be rewritten as

$$\ddot{Z}(t) + C\dot{Z}(t) + \Omega Z(t) = \Gamma \Theta^{\text{act}} V(t) + D, \tag{25}$$

where $Z(t) = [\eta_1, \eta_2, \eta_3]^{\text{T}}$, C is the experimentally determined damping co-efficient matrix of the plate and $C = \text{diag}\{90, 100, 100\}$, Ω is the natural frequency matrix and $\Omega = \text{diag}\{\omega_1^2, \omega_2^2, \omega_3^2\}$, Γ is the 3 by 3 matrix of actuator forces (see Ref. [1]) that will be defined below, $\Theta^{\text{act}} = \text{diag}\{\theta_1^{\text{act}}, \theta_2^{\text{act}}, \theta_3^{\text{act}}\}$, $V(t)$ is the input voltage vector to the three actuators given as $V(t) = [v_1(t), v_2(t), v_3(t)]^{\text{T}}$, and the 3×1 vector D is the external disturbance. Here,

$$\Gamma = \begin{bmatrix} 0.130 & 0.0779 & 0.0779 \\ 0 & -0.280 & 0 \\ 0 & 0 & 0.280 \end{bmatrix}. \tag{26}$$

Γ shows that the first patch only affect the first mode, while the second and third patches affect there respective modes as well as the first mode. The parameters $\theta_1^{\text{act}}, \theta_2^{\text{act}}$, and θ_3^{act} are the unknown nonlinear parameters that encompass the bonding, actuator and temperature uncertainties and estimated experimentally. The estimation of the damping coefficients and the nonlinear parameters was done by injecting a sinusoid of known voltage into each actuator and recording the resulting modal displacement and phase response.

The injection signal is swept over frequency to give an experimental frequency response of the system. Next the frequency response of Eq. (25) is fit to this data using a simple least squares fit with Θ^{act} and C as the independent variables. Fig. 3 depicts the results of the fitting procedure used to estimate Θ^{act} and C. In the figure, the horizontal axis is the frequency ratio $\omega_{\text{dr}}/\omega_i$ where ω_{dr} is the driving frequency. The vertical axis is the ratio $A\omega_{\text{dr}}^2/F$ where A is the amplitude of the response and F is the amplitude of the actuator input. The values of the parameters Θ^{act} for the three actuators at room temperature were found to be 0.071, 0.054, and 0.052.

The actuator placement depicted in Fig. 2 causes the first mode to be affected by all actuators. However, in the control design the effect of the second and third actuators on the first mode will be combined with the noise disturbance. As a result of this assumption Γ becomes a diagonal matrix in the control design decoupling

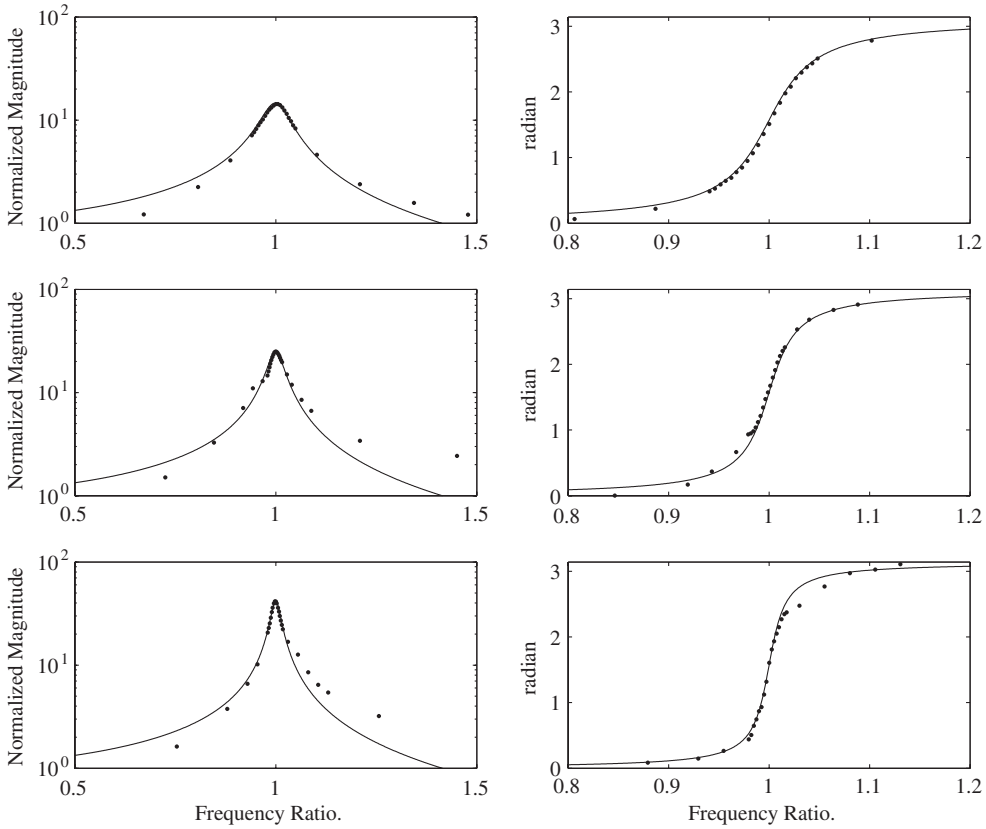

Fig. 3. Open-loop plate response. Measured data is shown with circular markers, model is shown with a solid line. (a) Magnitude and phase of Mode 1, Actuator 1, (b) Mode 2, Actuator 2, (c) Mode 3, Actuator 3.

the three equations ($\Gamma = \text{diag}\{\gamma_1, \gamma_2, \gamma_3\}$). The controllers need to be designed to handle the uncertainty in Ω and C and the nonlinearity of Θ^{act}.

4.2. H_∞ and adaptive control for three modes

4.2.1. H_∞ control

The same design process that was used in Ref. [1] and adopted from Refs. [7,8] is used here. Eq. (25) can be written in state-space form as

$$\dot{X} = A_p X + B_1 p D + B_2 p V, \tag{27}$$

$$Y = C_p X + D_p D, \tag{28}$$

where $X = [Z, \dot{Z}]^{\text{T}}$ is the state vector, D is the disturbance. In addition the plant matrices are given by

$$A = \begin{bmatrix} \mathbf{0} & I \\ \Omega & C \end{bmatrix}, \quad B_{1p} = \begin{bmatrix} \mathbf{0} \\ I \end{bmatrix}, \quad B_{2p} = \begin{bmatrix} \mathbf{0} \\ \Gamma \end{bmatrix}, \quad C_p = [\mathbf{0} \quad I], \tag{29}$$

where I is the 3×3 identity matrix. Note that B_{2p} does not include the nonlinear term Θ^{act}. The design of the H_∞ controller requires a linear plant so $\Theta^{\text{act}} = I$.

The H_∞ design weights chosen to shape the three controllers are given in Table 3. Note that the weights chosen for the second and third modes are the same. The block diagram for the design phase is given in Fig. 4.

Table 3
Weights for the H_∞ controller

Mode	W_1	W_2	W_3	W_4
1	10	5×10^{-6}	$\frac{3 \times 10^5}{7.16 \times 10^{-4}s + 1}$	$\frac{7.46 \times 10^{-5}s + 0.3125}{2.5 \times 10^{-8}s + 1}$
2,3	10	1.1×10^{-4}	$\frac{6 \times 10^4}{3.99 \times 10^{-4}s + 1}$	$\frac{6.64 \times 10^{-6}s + 0.0625}{2.5 \times 10^{-8}s + 1}$

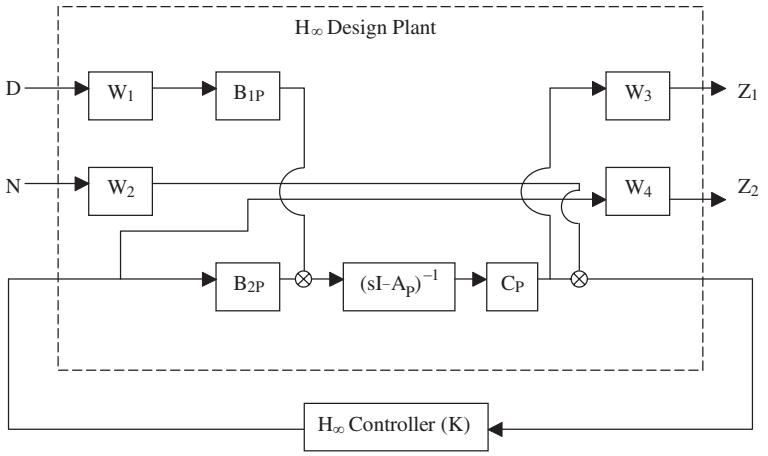

Fig. 4. Block diagram for the design of the H_∞ controller.

The controllers resulting from the design are linear and can be described by

$$\dot{X}_i = A_i X_i + B_i u_i, \quad i = 1, 2, 3, \tag{30}$$

$$v_i = C_i X_i + D_i u_i, \quad i = 1, 2, 3, \tag{31}$$

where X_i is the state of the controller, u_i is the input to the controller (the velocity of each mode), v_i is the output voltage of the actuator, and A_i, B_i, C_i, and D_i are matrices given by

$$A_1 = \begin{bmatrix} 0.000, & 1.555, & 5.861 \times 10^4, & 0 \\ -1.361 \times 10^6, & -3.446 \times 10^3, & -2.156 \times 10^7, & 5.211 \times 10^6 \\ 1.045 \times 10^1, & 8.767 \times 10^{-3}, & -9.548 \times 10^2, & 0 \\ -5.054 \times 10^4, & -2.427 \times 10^1, & -2.348 \times 10^6, & -2.010 \times 10^4 \end{bmatrix}, \tag{32}$$

$$B_1 = \begin{bmatrix} -1.518 \times 10^5 \\ 9.201 \times 10^8 \\ -2.399 \times 10^3 \\ 0 \end{bmatrix}, \tag{33}$$

$$C_1 = [-1.847 \times 10^{-1}, \quad -8.867 \times 10^{-5}, \quad -8.580, \quad 1.461 \times 10^2], \tag{34}$$

$$D_1 = [0], \tag{35}$$

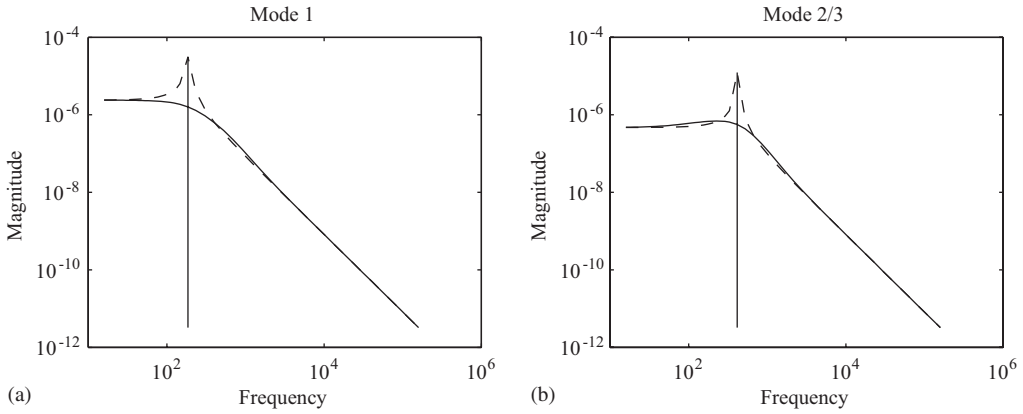

Fig. 5. Frequency response of the H_∞ controller. Dashed curve for the original system; solid curve for the closed-loop system; vertical line denotes modal frequency. (a) Mode 1, (b) Mode 2/3.

$$A_{2,3} = \begin{bmatrix} 0.000, & 1.054, & 3.615 \times 10^4, & 0 \\ -6.837 \times 10^6, & -7.316 \times 10^3, & -2.457 \times 10^7, & -1.121 \times 10^7 \\ 1.038 \times 10^1, & 2.082 \times 10^{-3}, & -3.024 \times 10^3, & 0 \\ -1.440 \times 10^3, & 3.625, & 6.196 \times 10^4, & -1.364 \times 10^4 \end{bmatrix}, \tag{36}$$

$$B_{2,3} = \begin{bmatrix} -6.220 \times 10^3 \\ 8.338 \times 10^8 \\ -2.399 \times 10^2 \\ 0 \end{bmatrix}, \tag{37}$$

$$C_{2,3} = [-1.249 \times 10^{-2}, \quad 3.146 \times 10^{-5}, \quad 5.376 \times 10^{-1}, \quad 3.470 \times 10^2], \tag{38}$$

$$D_{2,3} = [0]. \tag{39}$$

Simulation of the numerical model results in significant amplitude reductions as shown in Fig. 5.

4.2.2. Adaptive control

Three adaptive controllers were designed using the adaptive algorithm given in Section 3. Depending on which actuator is being excited, each controller will estimate θ_1^{act}, θ_2^{act}, or θ_3^{act} to get θ_1^{est}, θ_2^{est}, and θ_3^{est}. Again, the second and third controllers will be identical. All of the controllers will use the first modal equation as their reference model (each patch will excite the first mode). From Eq. (25),

$$\ddot{\eta}_1(t) + c_1\dot{\eta}_1(t) + \omega_1^2\eta_1(t) = \begin{bmatrix} 1 \\ 0 \\ 0 \end{bmatrix} \Gamma\Theta^{act} V(t). \tag{40}$$

Each controller excites the actuator with a 30 V, 150 Hz sinusoidal signal. For all the controllers, $g = 0.001$.

In order to effectively use the H_∞ controller, the plant must be linearized to match the plant used in its design (where $\Theta^{act} = I$). To do this, the H_∞ control voltage will be multiplied by the inverse of the parameter estimation Θ^{est}. The right-hand side of Eq. (25) then becomes $\Gamma\Theta^{act}\Theta^{est-1}V(t) + D$, where $\Theta^{est} = \text{diag}\{\theta_1^{est}, \theta_2^{est}, \text{ and } \theta_3^{est}\}$. If the estimation is perfect the right-hand side becomes $\Gamma V(t) + D$, which was the plant used in the H_∞ control design.

4.2.3. Simulation results

The controller was simulated on a system that closely matched the experimental setup, including the time delay of the system. In addition, a controller sampling rate of 10 kHz was used in the simulation. Because of the delays at higher frequencies (>2 kHz), high-frequency dynamics were excited. As a result, the gains in the simulations were reduced to prevent the excitation of the high-frequency dynamics. To better approximate the experimental conditions, the adaptive controller was run separately from the H_∞ controller. The adaptive parameter was estimated and applied to the voltage of the H_∞ controller. Fig. 6 shows the convergence of the adaptive parameters. The frequency of the disturbance was swept from 100 Hz to 1 kHz and the modal positions were recorded. The controller reduced the vibrations by 10 dB for the first mode and 8.2 dB for the second and third modes. Five additional simulations were run to test the range of the controller by varying Z by $\pm 10\%$, C by $\pm 50\%$ and $0.02\,\gamma_1 \leqslant \gamma_1^{\text{test}} \leqslant 0.05\,\gamma_1$, $0.01\,\gamma_2 \leqslant \gamma_2^{\text{test}} \leqslant 0.03\,\gamma_2$, and $0.01\,\gamma_3 \leqslant \gamma_3^{\text{test}} \leqslant 0.03\,\gamma_3$. The second test maximized all three parameters. The third test set Z and C to their minimum values and Γ to its maximum. The fourth test set Z and C to their nominal values and Γ to its minimum. Test five minimized all three parameters. The final test maximized Z and C and minimized Γ. Fig. 7 shows the results of the variations. The worst case reduction was 8.4 dB for the first mode and 7.3 dB for the second and third modes. These resulted from a 10% increase in modal frequency and a 50% increase in damping.

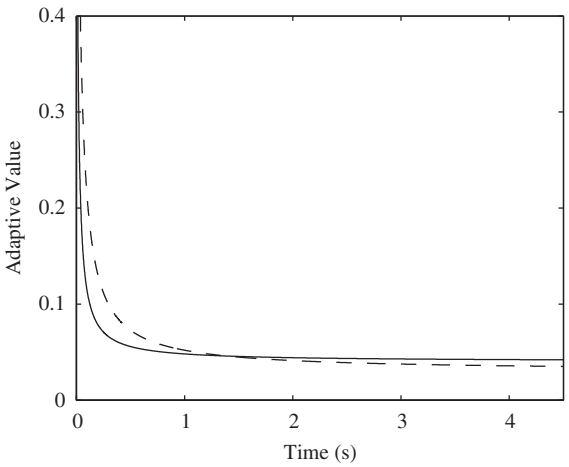

Fig. 6. Theoretical parameter convergence for the three distributed strain actuators. Solid curve for first actuator; dashed curve for the second and third actuators.

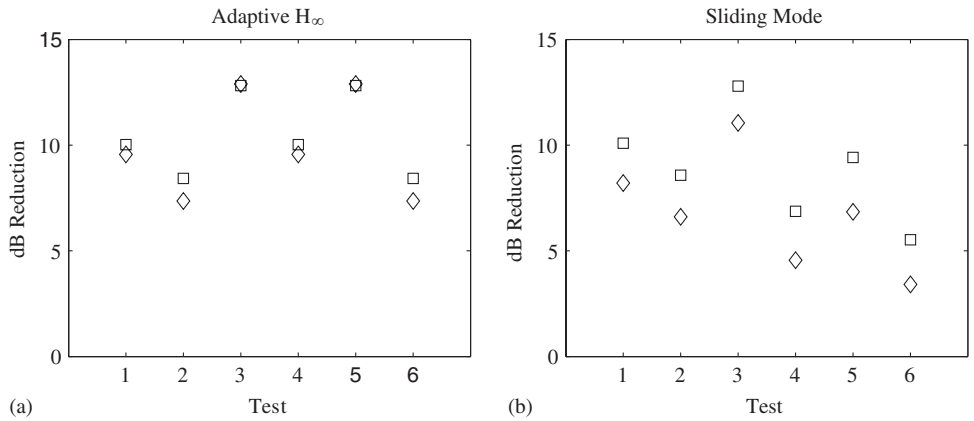

Fig. 7. Modal reduction of the H_∞ and sliding mode controllers. Square markers for mode 1; diamond markers for modes 2 and 3. Test conditions are: 1—nominal condition; 2—$1.1\omega_m$, $1.5C_m$, max k_f; 3—$0.9\omega_m, 0.5C_m$, max k_f; 4—$1.0\omega_m, 1.0C_m$, min k_f; 5—$0.9\omega_m, 0.5C_m$, min k_f; 6—$1.1\omega_m, 1.5C_m$, min k_f. (a) Adaptive H_∞, (b) Sliding mode.

4.3. Sliding mode control for three modes

4.3.1. Sliding mode control

The sliding mode controller is a transformation that reduces the system down to a first-order system, the sliding surface. Controlling this first-order system is simpler than controlling the original plant. If this sliding surface can be controlled, then the original system will be controlled.

From Ref. [6], Eq. (6) is rewritten as

$$\ddot{Z}(t) = f + \Gamma^* V, \tag{41}$$

where $f = -C\dot{Z} - \Omega Z$. Also, the external forces can be expressed as $[N_1, N_2, N_3]^{\mathrm{T}} = \Gamma^* V$, with $\Gamma^* = \mathrm{diag}\{\gamma_1^*, \gamma_2^*, \gamma_3^*\}$. The uncertainties on C and $\sqrt{\Omega_n}$ are estimated to be 50% and 10%, respectively. The range of the components of Γ^* are defined such that $0.02\,\gamma_1 \leqslant \gamma_1^* \leqslant 0.05\,\gamma_1$, $0.01\,\gamma_2 \leqslant \gamma_2^* \leqslant 0.03\,\gamma_2$, and $0.01\,\gamma_3 \leqslant \gamma_3^* \leqslant 0.03\,\gamma_3$. These limits were chosen based on experimental observation. Accordingly, the nominal value of f, $\hat{f}$, can be written as

$$\hat{f} = -\hat{C}\dot{Z} - \hat{\Omega} Z, \tag{42}$$

where $\hat{C}$ and $\hat{\Omega}$ are the nominal values of their respective matrices. Now, the estimation error, $|\hat{f} - f|$, can be bound by some function $\tilde{f}$:

$$\tilde{f} = 0.5C|\dot{Z}| + 0.21\Omega|Z|. \tag{43}$$

To suppress the vibration, the sliding surface s is defined as

$$s = \dot{Z} + \Lambda Z, \tag{44}$$

where $\Lambda = \mathrm{diag}\{\lambda_1, \lambda_2, \lambda_3\}$, with $\lambda_i > 0$. Then,

$$\dot{s} = \ddot{Z} + \Lambda\dot{Z} = f + \Gamma^* V + \Lambda\dot{Z}. \tag{45}$$

Vibration suppression is achieved when $s \to 0$ and $\dot{s} \to 0$. Bearing in mind that Eqs. (44) and (45) are completely decoupled, the following condition can be set:

$$\frac{1}{2}\frac{\mathrm{d}}{\mathrm{d}t}s_i^2 \leqslant -N|s_i|, \quad i = 1, 2, 3 \tag{46}$$

or

$$s_i\dot{s}_i \leqslant -N|s_i|, \quad i = 1, 2, 3, \tag{47}$$

for some $N > 0$.

Using Filippov's construction [6] for the equivalent dynamics,

$$\hat{v}_i = -\hat{f}_i - \lambda_i\dot{\eta}_i, \tag{48}$$

where $\hat{v}_i$ are the three components of the equivalent control vector. Thus, the control input is

$$v_i = \frac{\hat{v}_i}{\hat{\gamma}_i} - \frac{k_i}{\hat{\gamma}_i}\mathrm{sgn}(s_i), \quad i = 1, 2, 3, \tag{49}$$

where $\hat{\gamma}_i$ are the nominal values of γ_i (they will be specified below), $K = [k_1, k_2, k_3]^{\mathrm{T}}$ is the control gain vector, and sgn(s) is the signum function. Using Eqs. (45) and (47),

$$\left[f_i - \frac{\gamma_i^*}{\hat{\gamma}_i}\hat{f}_i + \lambda_i\dot{\eta}_i - \frac{\gamma_i^*}{\hat{\gamma}_i}\lambda_i\dot{\eta}_i - \frac{\gamma_i^*}{\hat{\gamma}_i}k_i\,\mathrm{sgn}(s_i)\right]s_i \leqslant -N|s_i|. \tag{50}$$

Therefore,

$$k_i \geqslant \frac{\gamma_i^*}{\hat{\gamma}_i}N \pm \left(\frac{\gamma_i^*}{\hat{\gamma}_i}f_i - \hat{f}_i\right) + \left(\frac{\gamma_i^*}{\hat{\gamma}_i}\lambda_i - \lambda_i\right)\dot{\eta}_i. \tag{51}$$

Here, $\hat{\gamma}_i$ are chosen to be $\hat{\gamma}_i = \sqrt{\min(\gamma_i^*)\max(\gamma_i^*)}$, such that

$$\beta_i^{-1} \leqslant \frac{\hat{\gamma}_i}{\gamma_i^*} \leqslant \beta_i, \tag{52}$$

where $\beta_i = \sqrt{\max(\gamma_i^*)/\min(\gamma_i^*)}$. Given the bounds above, k_i can be chosen to be

$$k_i = \beta_i N + \beta_i \tilde{f}_i + (\beta_i - 1)\lambda_i |\dot{\eta}_i|. \tag{53}$$

The design coefficients, λ_i and N, are chosen to be 5 and 10, respectively.

To avoid chatter, the sliding mode controller can be modified such that the signum function in Eq. (49) is replaced with a saturation function of the form

$$\mathrm{Sat}\left(\frac{s_i}{\Phi}\right) = \begin{cases} 1, & \text{if } s_i > \Phi, \\ -1, & \text{if } s_i < -\Phi, \\ s_i, & \text{otherwise.} \end{cases} \tag{54}$$

Eq. (49) then becomes

$$v_i = \frac{\hat{v}_i}{\hat{\gamma}_i} - \frac{k_i}{\hat{\gamma}_i}\mathrm{Sat}(s_i), \quad i = 1, 2, 3. \tag{55}$$

For simulation and experimental studies, Φ was chosen to be 0.001.

4.3.2. Simulation results

The sliding mode controller was tested in the same way as the H_∞ controller. The frequency of the disturbance was swept from 100 Hz to 1 kHz and the modal positions were recorded. The controller reduced the vibrations by 10 dB for the first mode and 8.2 dB for the second and third modes. Next, Ω, C and Γ were varied to test the range of the controller. Fig. 7(b) shows the results of the tests. The worst case reduction was 5.5 dB for the first mode and 3.4 dB for the second and third modes. These resulted from a 10% increase in modal frequency, a 50% increase in damping, and using the minimum values of γ (the weakest actuator).

5. Experimental results

The experimental setup is based on a 150 MHz floating point DSP, the TI6711. The disturbance to the plate was generated by a speaker over the plate. The acceleration at four locations on the plate were measured. The acceleration was sent through a 8 kHz second-order butterworth filter to remove aliasing effects by the analog-to-digital converters (ADCs). The signals were then sent through the ADCs to the DSP. The actuator voltage was sent out of the DSP through DACs, amplified and then sent to the distributed strain actuators. The speaker and plate are enclosed in a Thermotron temperature chamber that allows for controlled temperature tests. The experimental setup is shown in Figs. 8 and 9.

Since the controls use modal acceleration, velocity and position in their calculations, this information must be calculated from the measured plate accelerations. Assuming only the first four modes are present (we assume the fourth mode is present but uncontrolled) the modal acceleration can be extracted from the measured acceleration by evaluating the coordinate functions, Eq. (3) at the specific locations where the accelerometers are located. The coordinate function for the fourth mode can be found in Ref. [1]. The coordinate functions can then be solved given the positions of the accelerometers in the experimental setup. Each accelerometer measurement is made up of the four modal accelerations. Solving for the four model accelerations, we get

$$\ddot{\eta}_1 = 0.0557a_1 + 0.0717a_2 + 0.0717a_3 - 0.0557a_4, \tag{56}$$

$$\ddot{\eta}_2 = -0.0374a_1 + 0.0482a_2 - 0.0482a_3 + 0.0374a_4, \tag{57}$$

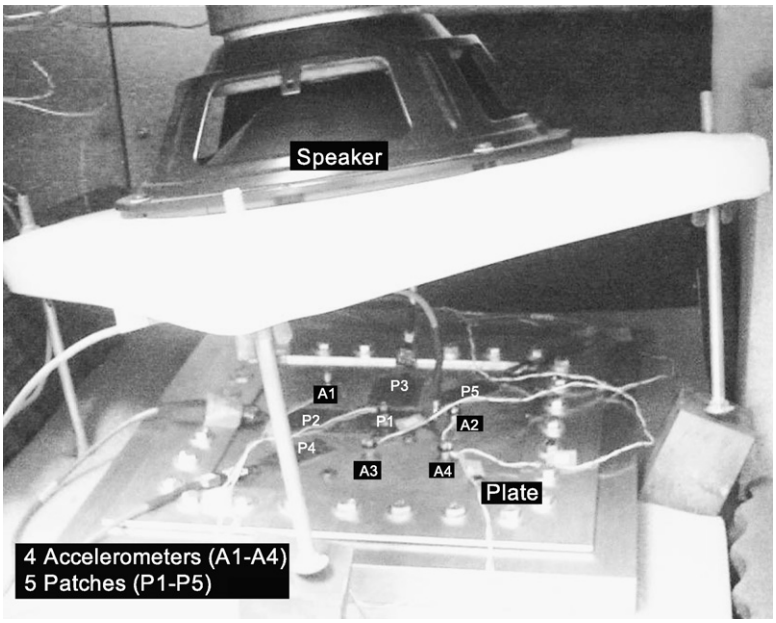

Fig. 8. Plate with detecting and actuation hardware. Note patches P4 and P5 are not used in these experiments.

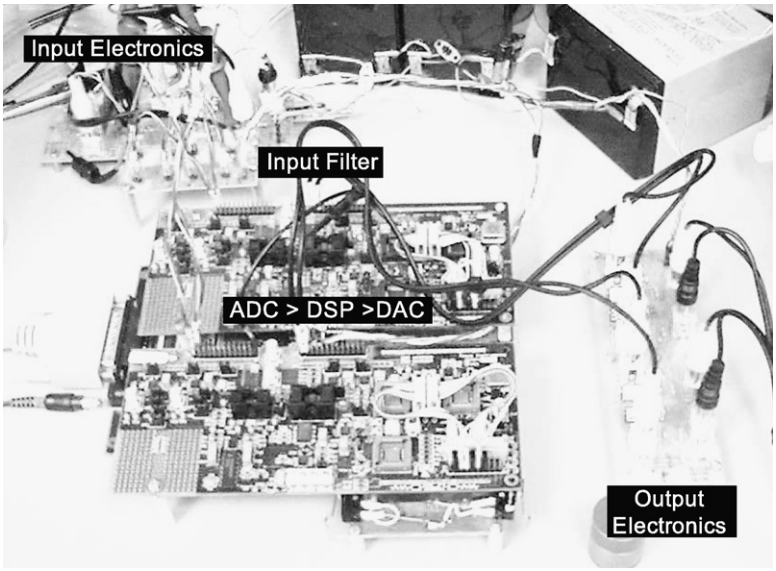

Fig. 9. Electronic hardware for control of three modes.

$$\ddot{\eta}_3 = 0.0374a_1 + 0.0482a_2 - 0.0482a_3 - 0.0374a_4, \tag{58}$$

$$\ddot{\eta}_4 = -0.0242a_1 + 0.0334a_2 + 0.0334a_3 - 0.0761a_4, \tag{59}$$

where a_i are the measured accelerations of the plate (see Fig. 2).

When testing the H_∞ controller, the adaptive parameter estimator was run first. The adaptive parameter found was fed into the H_∞ controller and its gain adjusted. Fig. 10 depicts the adaptive parameter convergence for test 1 (the behavior is qualitatively similar for all tests). This data was taken at room temperature. When compared with the model, the parameter convergence was virtually identical.

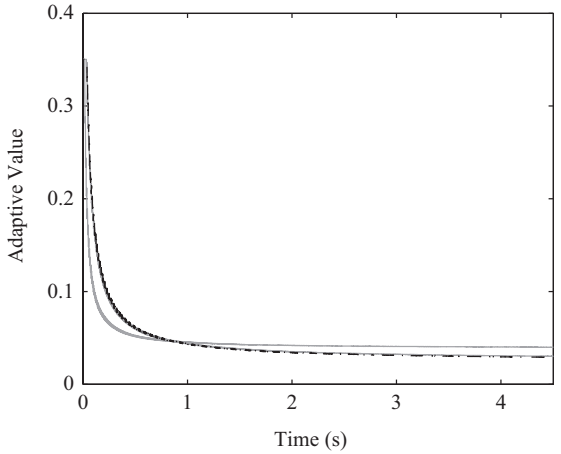

Fig. 10. Experimental parameter convergence for the first three distributed strain actuators. Dotted line for parameter 1; solid lines for parameter 2 and 3; dot-dashed line for parameter 3. The convergence for 2 and 3 are almost identical and the lines lie virtually on top of each other.

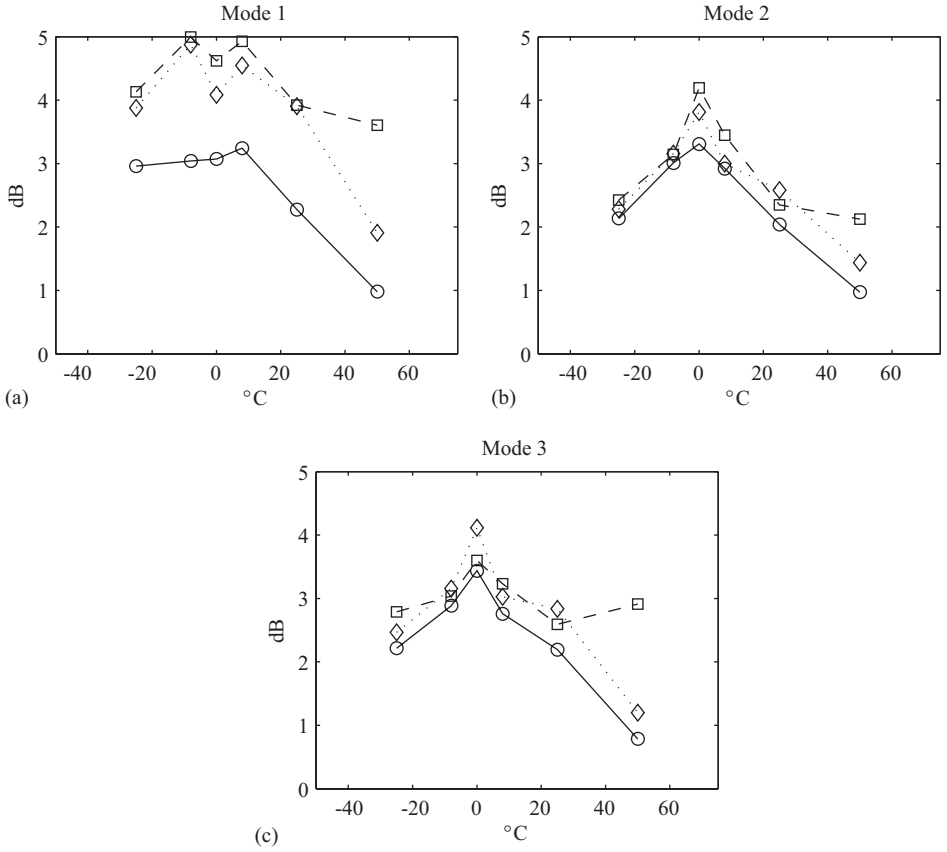

Fig. 11. Experimental vibration suppression of the three controllers. Solid line with circular markers for PVF; dashed line with square markers for H_∞; dotted line with diamond markers for sliding mode. (a) Mode 1, (b) Mode 2, (c) Mode 3.

The experimental results for the H_∞ controller with the adaptive parameter identification and the sliding mode controller are compared with a baseline positive velocity feedback controller. The controllers were tuned at the lowest temperatures because high-frequency noise had the greatest effect at low temperatures.

A sinusoidal disturbance was swept from 100 Hz to 1 kHz and the corresponding modal positions were recorded for the three controllers and for open-loop condition. The positive velocity feedback performed the worst of the three controllers. Its performance degraded over the temperature range, with significant performance loss at the high temperatures. The sliding mode controller performed better, but still degraded at higher temperatures. The H_∞ controller with the adaptive estimator was fairly consistent over temperature changes and had minor degradation at high temperatures. The reductions at the three modal frequencies are shown in Fig. 11.

6. Conclusions

In this paper, vibration suppression of a small square plate clamped on all edges was considered. Two control designs (H_∞ and sliding mode control) were presented to account for both model uncertainties and nonlinear effects due to temperature variations, bonding issues, and the actuator coating. These control methods were able to significantly reduce the vibrations over a wide range of tests. The H_∞ controller with the parameter estimation performed better across variations of the plant. However, that performance comes with a higher computational cost and a need to inject a signal into the actuator voltage periodically (for persistent excitation). The experimental results were not as good as the theoretical results because the gain of the controllers had to be reduced to prevent saturation of the accelerometers. Saturation due to high-frequency noise and the digitizing effects of the DAC were not accurately modelled. The delay of the system was approximately 0.23 ms. This corresponds to 180° phase shift at 2.2 kHz. If high-frequency noise is excited at 2.2 kHz, it will be amplified. A small displacement will correspond to a large acceleration, saturating the accelerometers. This was seen in experiments and the gain had to be reduced to prevent this. The degradation in performance between the ideal system and the actual system was not seen in other research because the time delay of controlled systems below 75 Hz is negligible. The experimental issues of controlling a higher-frequency system become more complex and have a greater effect on the system. Although some possible improvements can be taken (such as using parallel DSPs for each controller), time delay will continue to be a factor in the performance.

Acknowledgements

The authors would like to thank Raytheon Aircraft Integration Systems for partial funding of this research.

References

[1] P. Shimon, E. Richer, Y. Hurmuzlu, Theoretical and experimental study of efficient control of vibrations in a clamped square plate, *Journal of Sound and Vibration* 282 (2005) 453–473.
[2] L. Meirovitch, *Principles and Techniques of Vibrations*, Prentice-Hall, Inc., Upper Saddle River, NJ, 1997.
[3] E. Richer, Using Innovative Control Algorithms for Better Design of Force Actuators, PhD Dissertation, Southern Methodist University, 1999.
[4] A. Dimarogonas, *Vibrations for Engineers*, Prentice-Hall, Inc., Upper Saddle River, NJ, 1996.
[5] S. Sastry, M. Bodson, *Adaptive Control: Stability, Convergence, and Robustness*, Prentice-Hall, Englewood Cliffs, NJ, 1989.
[6] J.-J. Slotine, W. Li, *Applied Nonlinear Control*, Prentice-Hall, Inc., Upper Saddle River, NJ, 1991.
[7] R.T. Stefani, C.J. Savant Jr., B. Shahian, G.H. Hostetter, *Design of Feedback Control Systems*, Saunders College Publishing, Orlando, FL, 1994.
[8] K. Zhou, J.C. Doyle, *Essentials of Robust Control*, Prentice-Hall, Inc., Upper Saddle River, NJ, 1998.